

# Role of autophagy machinery dysregulation in bacterial chondronecrosis with osteomyelitis

Alison Ramser <sup>\*,†</sup>, Elizabeth Greene,<sup>\*</sup> Adnan A. K. Alrubaye,<sup>\*,†</sup> Robert Wideman,<sup>\*</sup> and Sami Dridi<sup>\*,†,1</sup>

<sup>\*</sup>Center of Excellence for Poultry Science, University of Arkansas, Fayetteville, AR 72701, USA; and <sup>†</sup>Cell and Molecular Biology, University of Arkansas, Fayetteville, AR 72701, USA

**ABSTRACT** Autophagy is a cell survival and homeostasis mechanism involving lysosomal degradation of cellular components and foreign bodies. It plays a role in bone homeostasis, skeletal diseases, and bacterial infections as both a cell-survival or cell-death pathway. This study sought to determine if autophagy played a role in bacterial chondronecrosis with osteomyelitis (BCO). BCO is a prominent cause of lameness in modern broilers and results from bacterial infection of mechanically stressed leg bone growth plates. The protein and gene expression of key autophagy machinery was analyzed in both normal and BCO-affected broilers using real-time qPCR and immunoblot, respectively. Gene expression showed a significant downregulation of key target

signatures involved in every stage of autophagy in BCO-affected bone, such as ATG13, SQSTM1 (p62), ATG9B, ATG16L, ATG12, LC3C, and RAB7A. Additionally, protein expression for LC3 was also significantly lower in BCO. An in vitro study using human fetal osteoblast cells challenged with BCO isolate, *Staphylococcus agnetis* 908, showed a similar dysregulation of autophagy machinery along with a significant decrease in cell viability. When autophagy was inhibited via 3-methyladenine or chloroquine, comparable decreases in cell viability were seen along with dysregulation of autophagy machinery. Together, these results are the first to implicate autophagy machinery dysregulation in the pathology of BCO.

**Key words:** autophagy, broiler, bacterial chondronecrosis with osteomyelitis, lameness, osteoblast

2022 Poultry Science 101:101750

<https://doi.org/10.1016/j.psj.2022.101750>

## INTRODUCTION

Autophagy is a key component of cellular homeostasis, survival, defense, and death. It is a process by which cells are able to degrade cellular debris, damaged organelles, or foreign bodies, via membrane isolation coupled with lysosomal fusion and degradation (Klionsky, 2005; Deretic et al., 2013). There are 4 stages in autophagy, initiation, nucleation, elongation, and fusion (Noda et al., 2009). Initiation involves the activation of autophagy machinery. Nucleation is characterized by the sequestering of key proteins and complexes to the site of phagophore formation. Elongation occurs as the autophagosome expands and eventually closes. Fusion refers to the coalescence of the mature autophagosome with a lysosome to undergo lysosomal degradation of its contents (Hurley and Young, 2017; Nakamura and Yoshimori, 2017). Autophagy contributes to cellular survival through regular maintenance as well as defense

and aids in cellular processes and functions. In bone, functioning autophagy machinery is essential to bone growth and homeostasis via promotion of chondrocyte survival in hypoxic environments, regulation of osteoblast and osteoclast differentiation, and contribution to osteoblast mineralization (Onal et al., 2013; Shapiro et al., 2014; Piemontese et al., 2016; Li et al., 2018). Under bacterial challenge, autophagy's effectiveness increases cell survival and decreases bacterial loads (Amano et al., 2006; Cemama and Brumell, 2012; Maurer et al., 2015). While its ineffectiveness or inhibition has damaging effects on cellular viability and function. For example, some bacteria, such as *Staphylococcus aureus*, dysregulates autophagy via inhibition of fusion in order to evade the cellular defense and persist within the cell and ultimately causes cell death (Ogawa et al., 2011; Geng et al., 2020). It is the dynamic nature of autophagy's involvement in physiological states that has led it to be increasingly investigated in different diseases and disorders. In the case of bacterial chondronecrosis with osteomyelitis (BCO), the involvement of bacterial infection and bone inflammation as well as cellular necrosis make autophagy a pathway worth investigating given its significance to both the function of bone and response to bacteria.

Published by Elsevier Inc. on behalf of Poultry Science Association Inc. This is an open access article under the CC BY-NC-ND license (<http://creativecommons.org/licenses/by-nc-nd/4.0/>).

Received July 15, 2021.

Accepted January 23, 2022.

<sup>1</sup>Corresponding author: [dridi@uark.edu](mailto:dridi@uark.edu)

Bacterial chondronecrosis with osteomyelitis, also known as femur head necrosis, is a common cause of lameness in the modern broilers affecting fast-growing and higher yielding birds (Wideman et al., 2012). It is characterized by bacterial infection primarily in the proximal head of rapidly-growing leg bones of a broiler, resulting in chondronecrosis and osteomyelitis (Wideman and Prisby, 2012). It is theorized that collagen-binding bacteria, entering the bloodstream via the respiratory or gastrointestinal tract, are able to come into contact with preexisting wound sites within the mechanically-stressed, highly-vascularized growth plates and colonize (Al-Rubaye et al., 2015; Wideman, 2015). These wound sites also often transect blood supply leading to hypoxic conditions. As infection persists, inflammation and necrosis lead to bone attrition and associated lameness can become detectable, although subclinical BCO can also occur (Wideman and Prisby, 2012; Alrubaye et al., 2020). Understanding and combating BCO, and associated lameness, has become a high priority for improving both animal welfare and production.

Although it is now better understood how bacteria infect the bone and what the end-point symptoms of BCO are, the underlying mechanisms by which bacteria cause BCO still need to be fully defined. It has been shown that the mitochondrial dysfunction exists in BCO-affected tissue, but molecular pathways linking bacterial effects and what is seen in BCO tissue have yet to be discovered (Ferver et al., 2021). To that end, this study sought to elucidate the potential involvement of autophagy in BCO.

## MATERIALS AND METHODS

### Collection of BCO and Normal Bone Samples

All animal experiments were approved by the University of Arkansas (Fayetteville, AR) Animal Care and Use Committee (protocol number 15043) and were in accordance with recommendations in *NIH's Guide for the Care and Use of Laboratory Animals*. The BCO model and healthy counterparts were conducted as previously described (Wideman et al., 2012; Wideman and Prisby, 2012). Briefly, animals were placed on either litter or wire-flooring and had ad libitum access to fresh water and feed (3.9 Mcal metabolizable energy kg<sup>-1</sup> and 180 g crude protein kg<sup>-1</sup>) while the experiment took place at the University of Arkansas Poultry Research Farm. Ambient temperature was lowered gradually from 32°C to 25°C by 21 d of age. A light cycle of 23 h light/1 h dark was maintained along with an approximately 20% relative humidity until 56 d of age. At the end of the 56 d, animals were weighed, humanely euthanized, and immediately necropsied to determine presence of subclinical lesions in the proximal heads of both the femora and tibiae. Bone was selected macroscopically based on previously reported scale (Wideman et al., 2012; Wideman and Prisby, 2012). Normal bone was taken from animals raised on litter

only and when considered free of any necrosis or lesion and BCO-affected bone was from birds raised on wire-flooring and exhibiting lameness, and consisted of bone with femur head necrosis. Proximal portions of bone, primarily consisting of the growth plate, from both affected and unaffected animals were snap frozen in liquid nitrogen and stored at -80°C for later analysis.

### Cell Culture

Human fetal osteoblast (hFOB) 1.19 cells (CRL-11372; ATCC, Manassas, VA) were cultured in a 1:1 mixture of Ham's F12 medium/Dulbecco's modified Eagle's medium, 10% fetal bovine serum, and 0.3 mg/mL G418. Cells were grown at 34°C in a humidified atmosphere of 95% air and 5% CO<sub>2</sub> using either 6- or 96-well plates for molecular analyses and cell viability, respectively.

### Bacterial Challenge

*Staphylococcus agnetis* strain 908 (a generous gift from Dr. Douglas Roads, University of Arkansas) was isolated from the BCO-affected bone (Al-Rubaye et al., 2015), and was grown overnight in Luria broth at 37°C. To determine cell density, cultures were diluted using phosphate-buffered saline before absorbance at 650 nm was measured. Bacteria at a multiplicity of 50:1 were added to cell cultures in antibiotic-free media and left to attach for 1 h. Cells were washed 3 times with phosphate-buffer saline and complete media was added. Cells were maintained for an additional 24 h and then processed for protein isolation (Greene et al., 2019).

### Autophagy Inhibition

hFOB cells were treated with either 3-Methyladenine (3-MA) at a concentration of 5mM (Sigma Aldrich, St. Louis, MO), chloroquine (CQ) at a dose of 10 μM (InvivoGen, San Diego, CA), or vehicle control for 24 h before being lysed. Pilot studies were used to determine effective inhibitor dose.

### Cell Viability

Cell viability was performed as previously described (Dridi et al., 2012). Briefly, hFOB cells were seeded at  $1 \times 10^4$  cells per well of a 96-well plate before being infected as described above. CellTiter 96 AQueous One Solution CellProliferation Assay (Promega, Madison, WI) was used, according to manufacturer's recommendations, and results were obtained using a Synergy HT multimode microplate reader (BioTek, Winooski, VT). All sample readings were background corrected, and results were reported relative to control (n = 24/treatment).

## RNA Isolation, Reverse Transcription, and Real-time Quantitative PCR

From the normal and BCO-affected bone samples ( $n = 6/\text{group}$ ), total RNA was isolated in accordance with the protocol of (Carter et al., 2012). Cellular RNA was isolated using Trizol reagent (Life Technologies, Carlsbad, CA), based on manufacturer's instructions. RNA concentrations were determined using Synergy HT multimode microplate reader and total RNA was reverse transcribed using qScript cDNA SuperMix (Quanta Biosciences, Gaithersburg, MD). Amplification was achieved using Power SYBRGreen Master Mix (Life Technologies, Carlsbad, CA) and real-time quantitative PCR (7500 Real Time System; Applied Biosystems, Foster City, CA). The sequences for oligonucleotide primers for *r18s*, *Beclin1*, *ATG7*, *ATG3*, *LC3A*, *LC3B*, and *LC3C* were previously published (Piekarski et al., 2018; Piekarski-Welsher et al., 2018). As well as *ATG13*, *ATG9A*, *ATG14*, *UVRAG*, *ATG16L*, *ATG12*, *ATG4A*, *ATG4b*, and *ATG10* (Piekarski et al., 2014). Additional primers used were *ATG2B* (forward, 5'- CCGTTCCTCGGAG TCCATCA -3'; and reverse, 5'- GAGCCGGTGCCC TGGTA -3'), *ATG9B* (forward, 5'- TCACCCCTGAA-GATGGAGAGA -3'; and reverse, 5'- TTTCCAGCAT TGGCTCAATC -3'), *RAB7A* (forward, 5'- GTGC CAAGGAGGCCATTAAC -3'; and reverse, 5'- AAGTGCATTTTCGTGCAATCG -3'), *SQSTM1* (*p62*) (forward, 5'- TTACGTGCAGGACGGAGTTTT -3'; and reverse, 5'- CACGCCTGCACTCCTTTTTTC -3'), and *LAMP2* (forward, 5'- TCAATAGCTGAAGAAT GCTTTGCT -3'; and reverse, 5'- TGCCAACTGC-GACTGGAATA -3').

Real-time quantitative PCR cycling conditions were 50°C for 2 min, 95°C for 10 min and 40 cycles of a 2-step amplification (95°C for 15 s followed by 58°C for 1 min). The dissociation protocol from the sequence detection system was used for melting curve analysis to exclude potential contamination of nonspecific PCR products. Negative controls that were used as templates contained no reverse transcription products. Relative expression of target genes was determined using the  $2^{-\Delta\Delta C_T}$  method and healthy bone tissue or untreated cells were used as calibrators (Schmittgen and Livak, 2008).

## Western Blot Analysis

Bone samples and cell lysate were homogenized in lysis buffer (10 mmol/L Tris base, pH 7.4; 150 mmol/L NaCl; 1 mmol/L EDTA; 1 mmol/L EGTA; 0.1% Triton X-100; 0.5% Nonidet P-40; and protease and phosphatase inhibitors) and stainless-steel beads, using the Bullet Blender Storm (NextAdvance, Averill Park, NY). Total protein concentrations were determined using a Bradford assay kit (Bio-Rad, Hercules, CA), ran in 4 to 12% gradient Bis-Tris gels (Life Technologies) and then transferred to polyvinylidene difluoride membranes. Once transferred, membranes were blocked using a Tris-buffered saline (TBS) with 5% nonfat milk and Tween 20 at room temperature for 1 h. The membranes were

washed with TBS and Tween 20 and then incubated with primary antibodies at a dilution of either 1:500 or 1:1000 overnight at 4°C. Primary antibodies used were rabbit anti-Beclin1 (Cell Signaling Technology, Danvers, MA), rabbit anti-ATG7 (Cell Signaling Technology, Danvers, MA), rabbit anti-ATG16L (Aviva Systems Biology, San Diego, CA), rabbit anti-ATG12 (Cell Signaling Technology, Danvers, MA), rabbit anti-ATG3 (Thermo Fisher Scientific, Waltham, MA), rabbit anti-ATG5 (Cell Signaling Technology, Danvers, MA), rabbit anti-LC3 (Cell Signaling Technology, Danvers, MA), and rabbit anti-RAB7 (Santa Cruz Biotechnology, Dallas, TX). After another wash, secondary antibodies diluted to 1:5000 were added to 5% nonfat milk in TBS and Tween 20 and incubated with the membranes at room temperature for 1 h. The protein signals were visualized using chemiluminescence (ECL Plus; GE Healthcare, Pittsburg, PA) and images were captured using the FluorChem M MultiFluor System (ProteinSimple, San Jose, CA). Prestained molecular weight marker (Precision Plus Protein Dual Color) was used as a standard (Bio-Rad, Hercules, CA). Protein loading was assessed by immunoblotting using rabbit anti-glyceraldehyde-3-phosphate dehydrogenase (Santa Cruz Biotechnology, Dallas, TX). Image acquisition and analysis were performed by AlphaView software (version 3.4.0, 1993–2011; ProteinSimple). The relative levels of target autophagy proteins were normalized to glyceraldehyde-3-phosphate dehydrogenase.

## Statistical Analysis

Data were analyzed by Student *t* test or One-way ANOVA, as appropriate, using GraphPad version 7.03 (GraphPad Software, Inc., LaJolla, CA). Results are expressed as means  $\pm$  SEM, with *P*-value < 0.05 set as statistically significant.

## RESULTS

### The Expression of Key Autophagy markers was Downregulated in BCO-affected Tissues

Key autophagy machinery-associated genes, and corresponding proteins, involved in initiation were measured in normal and BCO-affected tissues. Both protein and gene expression were analyzed in normal and BCO affected femurs for Coiled-Coil Myosin-Like BCL2-Interacting Protein (Beclin1) with protein expression being significantly higher in BCO-affected bone, however, no significant difference was seen in gene expression (Figures 1A-1C) ( $P < 0.05$ ). Sequestosome I (*SQSTM1*), also known as Autophagy Receptor P62 (*p62*), also showed no significant differences in mRNA expression (Figure 1E). However, Autophagy-related protein 13 (*ATG13*) mRNA expression was significantly downregulated in BCO-affected tissue (Figures 1D and 1E) ( $P < 0.05$ ).

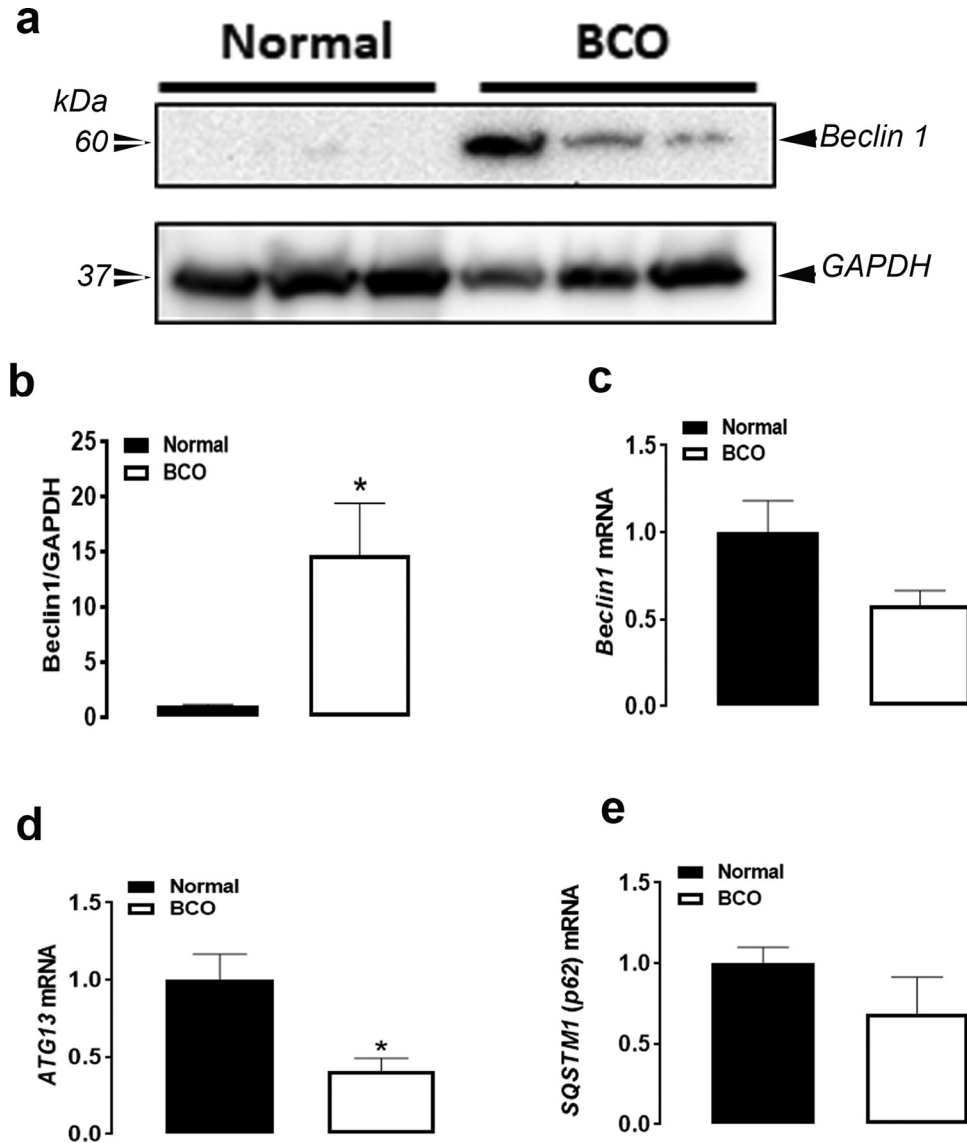


**Figure 1.** Dysregulation of autophagy initiation in BCO-affected Bone. Protein expression of Beclin1 was determined by Western blot (A, B). The expression of Beclin 1, ATG13, and SQSTM1 genes was measured by real-time quantitative PCR as described in materials and methods (C-E). Significance was determined using a student *t* test with *P*-value < 0.05. Data are means  $\pm$  SEM (*n* = 6) and the figure is a representative immunoblot. \* indicates significant difference between Normal and BCO. Abbreviation: BCO, bacterial chondronecrosis with osteomyelitis.

At the nucleation stage, Autophagy-related protein 5 (ATG5) protein expression was measured with no significant difference seen when comparing BCO-affected and normal bone (Figures 2A and 2B). However, the mRNA expression of ATG14 and ATG9B were significantly downregulated in BCO, when compared to normal bone (Figures 2C and 2E) (*P* < 0.05). Autophagy-related protein 9A mRNA expression showed no significant differences between normal and BCO-affected bone (Figure 2D).

The elongation stage of autophagy saw several significant differences in expression of autophagy molecular signatures. While protein expression of ATG7, ATG16L, ATG12, and ATG3 were not significantly different between BCO and normal bone, LC3 protein expression was significantly lower in BCO-affected bone (Figures 3A and 3F) (*P* < 0.05). Gene expression of ATG16L, ATG12, LC3C, ATG2B, ATG4B, and ATG10 were also significantly downregulated in BCO-affected bone compared to normal (Figures 3H, 3I, 3M,

3N, 3P, 3Q) (*P* < 0.05). ATG7, ATG3, LC3A, LC3B, and ATG4A showed no significant difference between BCO and normal tissue (Figures 3G, 3J, 3L, 3L, 3O).

Autophagy machinery involved in the fusion stage showed decreased mRNA abundances of member RAS Oncogene Family (RAB7A) in BCO-affected bone (Figure 4C) (*P* < 0.05). While protein expression of RAB7 as well as mRNA expression of Lysosomal Associated Membrane Protein 2 (LAMP2) and UV Radiation Resistance-Associated Gene (UVRAG) were not significantly different between normal and BCO (Figures 4A, 4B, 4D, 4E).

### ***S. agnetis* 908 Challenge Decreased Viability and Key Autophagy Machinery Expression in hFOB Cells**

Exposure to *S. agnetis* 908 resulted in significant decreased cell viability in hFOB cells (Figure 5A) (*P* <

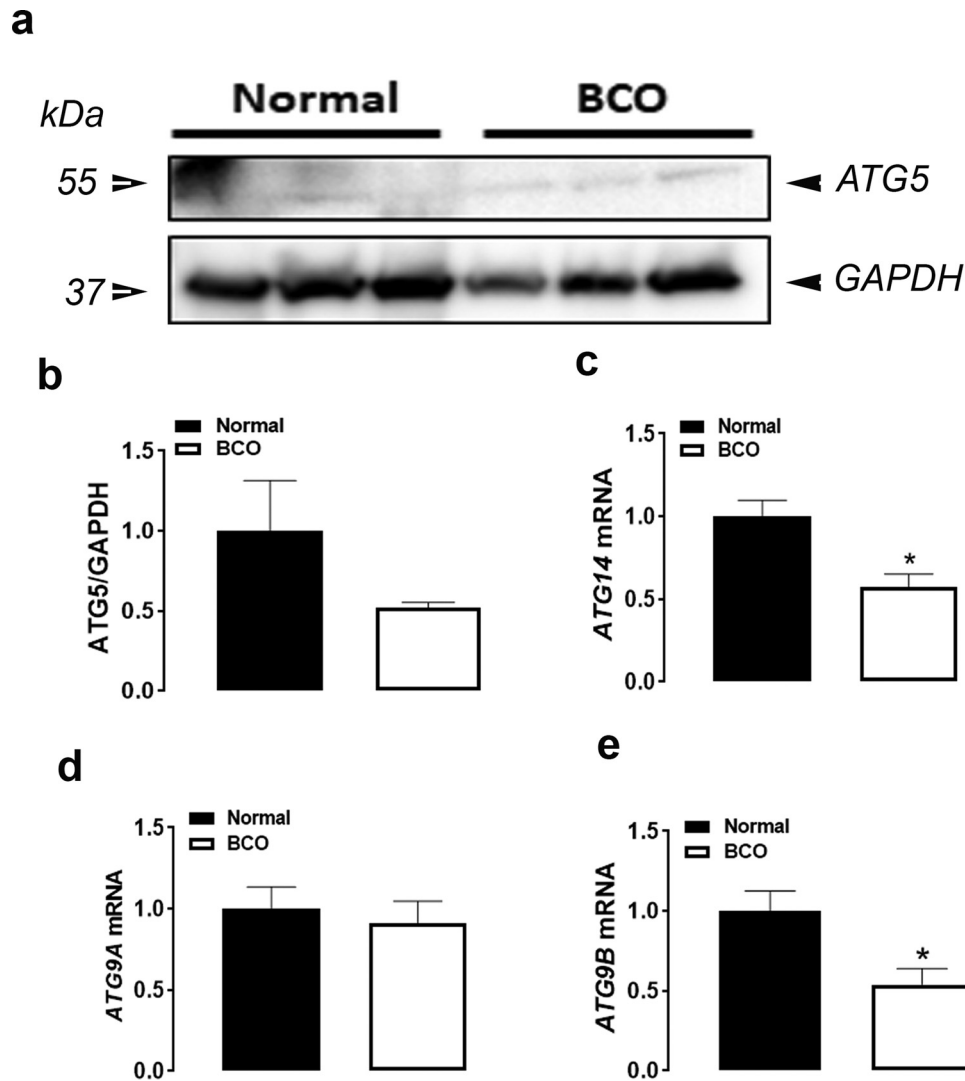


**Figure 2.** Autophagy nucleation machinery status in BCO-affected Bone. Protein expression for ATG5 (A) and statistical analysis of the immunoblot analyses (B). Gene expression for key nucleation machinery, *ATG14* (C), *ATG9A* (D), and *ATG9B* (E) was determined by qPCR. Significance was determined using a student *t* test with *P*-value < 0.05. Data are means  $\pm$  SEM (*n* = 6) and the figure is a representative immunoblot. \* indicates significant difference between normal and BCO. Abbreviation: BCO, bacterial chondronecrosis with osteomyelitis.

0.05). Protein expression of ATG7, ATG16L, Beclin1, ATG12 and ATG3 were significantly lower in bacterially challenged cells compared to control (Figures 5B-5E, 5G, 5H) (*P* < 0.05). The ratio of LC3 type II to LC3 type I was significantly increased in cells under bacterial challenge (Figures 5B and 5J) (*P* < 0.05). ATG5 and RAB7 protein expression were unaffected by exposure to *S. agnetis* 908 (Figures 5B, 5F, 5I).

### Inhibition of Autophagy Decreased hFOB Cell Viability and Autophagy Machinery Expression

Treatment of hFOB cells with either 3-MA or CQ resulted in significantly decreased cell viability in hFOB cells (Figure 6 A). Protein expression of ATG7 and Beclin1 was significantly decreased in cells exposed to both inhibitors compared to control (Figures 6B-6D). ATG12 and ATG3 protein levels were lower in cells treated with CQ compared to control, but not 3-MA

(Figures 6B, 6E, 6F) (*P* < 0.05). The ratio of LC3 type II to LC3 type I was significantly increased in both 3-MA- and CQ-treated hFOB cells, with CQ treatment resulting in the highest ratio (Figures 6B, 6G) (*P* < 0.05).

## DISCUSSION

In the pursuit of identifying potential mechanisms responsible for BCO, the autophagy pathway was investigated. Autophagy has been increasingly implicated in several skeletal disorders such as avascular necrosis of the femur head, glucocorticoid induced osteoporosis and osteomyelitis (Liu et al., 2014; Shen et al., 2018; Wang et al., 2019; Ichimiya et al., 2020; Zheng et al., 2020). In osteomyelitis, autophagy has been shown to be manipulated by causative agents allowing their persistence within the cell and subsequent cell death (Schnaith et al., 2007; Neumann et al., 2016). Its dual role in both cellular survival and cell death under bacterial challenge and bone homeostasis as well as its

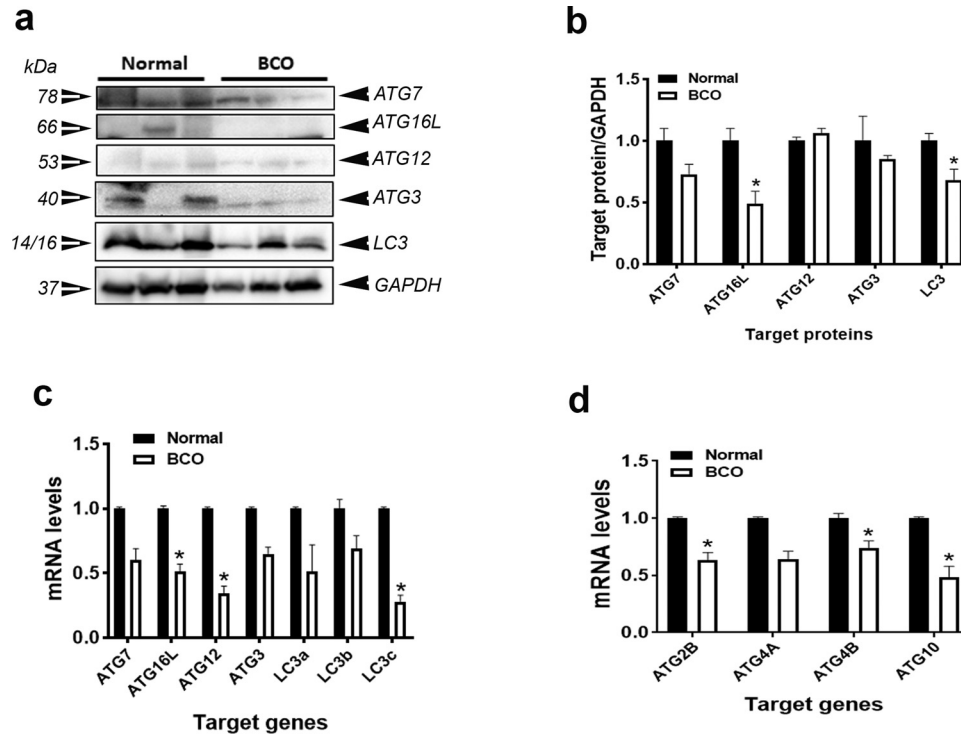


**Figure 3.** Alteration of autophagy elongation machinery in BCO-affected Bone. Protein expression for ATG7, ATG16L, ATG12, ATG3, and LC3 (A) and statistical analysis of the results as normalized to GAPDH (B). Gene expression for key elongation machinery, *ATG7*, *ATG16L*, *ATG12*, *ATG3*, *LC3A*, *LC3B*, and *LC3C* (C), *ATG2B*, *ATG4A*, *ATG4B*, and *ATG10* (D). Significance was determined using a student *t* test with *P*-value < 0.05. Data are means  $\pm$  SEM (*n* = 6) and the figure is a representative immunoblot. \* indicates significant difference between normal and BCO. Abbreviation: BCO, bacterial chondronecrosis with osteomyelitis.

susceptibility to bacterial manipulation, warrant the in-depth analysis of autophagy in BCO.

The initiation stage of autophagy has been shown to be affected under bacterial challenge, depending on the bacterium involved (Birmingham et al., 2006; Geng et al., 2020). A key component of autophagy initiation is formation of the ULK1 complex, which requires the involvement of ATG1 proteins such as ATG13 (Yamamoto et al., 2016; Zachari and Ganley, 2017; Chu et al., 2020). Bacterial chondronecrosis with osteomyelitis-affected femurs were shown to have significantly decreased mRNA expression of *ATG13*. Phosphorylation of ATG13 by mechanistic target of rapamycin complex 1 occurs under normal conditions, inhibiting autophagy (Bjørkøy et al., 2009). It is through the inactivation of mechanistic target of rapamycin complex 1 that stimuli, such as amino acid depletion and stress, activate the autophagy pathway within a cell (Desantis et al., 2015). Decreased expression of ATG13 indicates a potential inhibition of autophagy initiation. Another key component of autophagy initiation is the activation of the phosphoinositide 3-kinase (PI3K) class III complex which is dependent on the Bcl-2-Beclin1 complex (Houtman et al., 2019). Under normal conditions, Bcl-2 binds Beclin1 thereby inactivating PI3K complex and autophagy as a result (Esteves et al., 2019). It has been shown in cancer cells that inhibition of Beclin1 protein promotes autophagy (Li et al., 2013). However, in other cell types, such as microglia, increased expression of Beclin1 was coupled with apparently increased autophagic flux (Ke et al., 2019). In BCO

tissue, Beclin1 protein was significantly higher in BCO. Since BCO involves a bacterial component, it is worth noting that *Staphylococcus* species have been shown to induce autophagy initiation in order to become contained in the protective membrane before inhibiting later stages of autophagy (Lv et al., 2019). The downregulation of *ATG13* in BCO bone coupled with increased Beclin1 protein expression could be indicative of a dysregulation of autophagy initiation under BCO conditions potentially caused by bacterial influence.

Two key markers involved in autophagy nucleation were significantly downregulated in BCO-affected femurs, *ATG14* and *ATG9B*. ATG9 is believed to be involved in bringing lipids to the newly forming membrane in the phagophore assembly site (He et al., 2006; Zhuang et al., 2017; Sawa-Makarska et al., 2020). ATG9 is critical to survival of mice in the early neonatal starvation period in which functioning autophagy is essential (Kuma et al., 2004). In the case of bacterial infection, ATG9 has been shown to be essential in the formation of the double membrane around *Salmonella* (Kageyama et al., 2011). A dysregulation of ATG9 production under BCO conditions could point to disruptions in the autophagy pathway. ATG14 is a subunit of the PI3K complex I which aids in directing the complex to the phagophore assembly site where the complex plays a major role in membrane elongation of the forming autophagosome (Mei et al., 2016). Autophagy studies involving yeast and mammals have shown that overexpression of ATG14 increases autophagic activity (Matsunaga et al., 2010; Obara and Ohsumi, 2011).

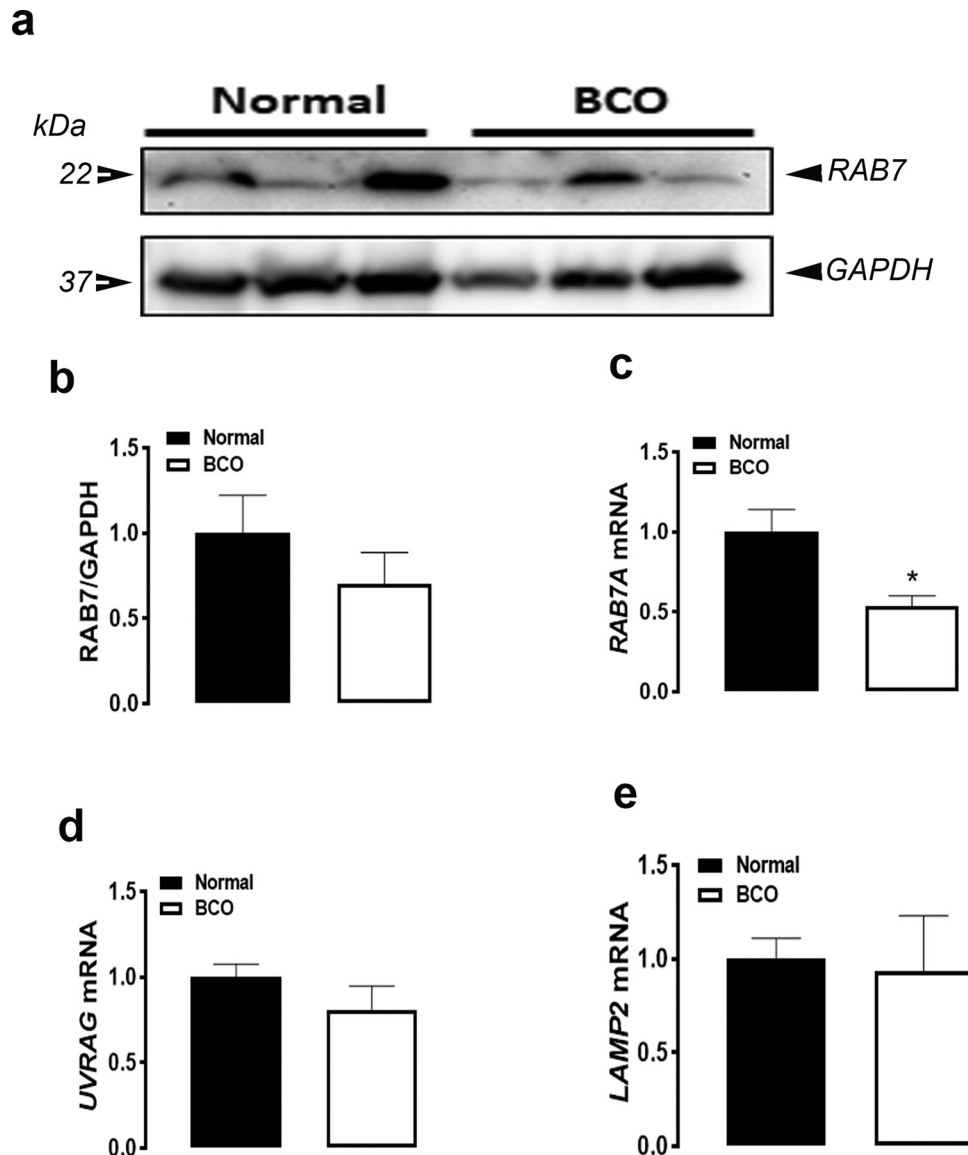


**Figure 4.** Dysregulation of autophagy fusion machinery in BCO-affected Bone. Protein expression for RAB7 (A) and corresponding statistical analysis (B) as normalized to GAPDH. Gene expression for *RAB7A* (C), *UVRAG* (D), and *LAMP2* (E), key autophagy fusion machinery, was measured by qPCR. Significance was determined using a student *t* test with *P*-value < 0.05. Data are means  $\pm$  SEM (n = 6) and the figure is a representative immunoblot. \* indicates significant difference between Normal and BCO. Abbreviation: BCO, bacterial chondronecrosis with osteomyelitis.

Additionally, deletion of ATG14 has been shown to affect the localization of other key autophagy machinery such as ATG8 and the ATG5-ATG12/ATG16L complex and, therefore, indirectly regulating autophagosome size (Abeliovich et al., 2000; Suzuki et al., 2007; Xie et al., 2008). Both ATG9 and ATG14 dysregulation in BCO bone suggest that the nucleation stage of autophagy may be affected under BCO conditions.

Elongation involves the expansion and closure of the phagophore to form an autophagosome. This process begins with the cleavage of LC3 by ATG4. LC3 is then conjugated from LC3 type I to membrane-bound LC3 type II by ATG7 and ATG3 (Döring et al., 2018). The ATG5-12/ATG16L complex comes into play again during elongation by recruiting ATG7 and ATG3 and forming the scaffold by which the maturing phagophore elongates and requires the activity of ATG7 and ATG10 (Nair et al., 2011). In BCO affected tissue, there was

significant decreased gene expression of *ATG12*, *ATG16L*, *LC3C*, and *ATG4B*. In the case of LC3, both LC3 protein and *LC3C* gene expression were significantly lower in BCO bone. Additionally, ATG2B and ATG10 were also significantly decreased. ATG2 acts as a tether between the preautophagosome membranes and the endoplasmic reticulum during elongation to aid in expansion and closure (Obara et al., 2008; Kotani et al., 2018). It has been shown that depletion of ATG2A and ATG2B leads to an accumulation of open and immature phagophore structures in mammalian cells (Velikkakath et al., 2012; Kishi-Itakura et al., 2014). The formation of the ATG5-ATG12 conjugation of the ATG5-ATG12/ATG16L complex is dependent on initial formation of an ATG12-ATG10 thioester intermediate (Han et al., 2019). Indeed, mutations in the ATG10 gene have shown to lead to dysfunction of the ATG5-ATG12 conjugation and lack of autophagic bodies

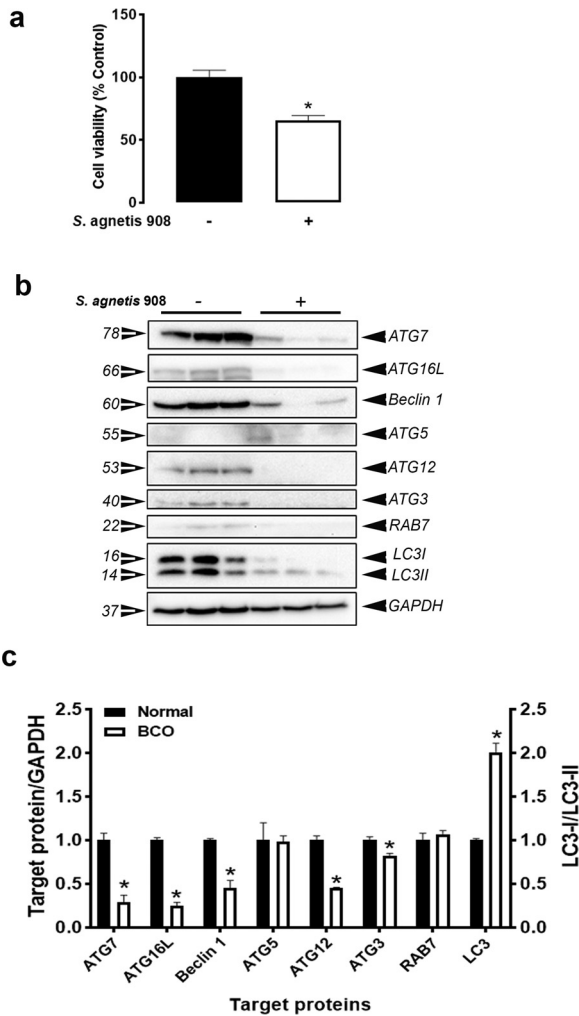


**Figure 5.** Effect of *Staphylococcus agnetis* 908 on cell viability and autophagy machinery in hFOB cells. MTT assay results from hFOB cells challenged with *S. agnetis* 908 at a MOI of 50:1 or a vehicle control for 24 h (A). Western blot results (B) and statistical analysis for ATG7, ATG16L, Beclin1, ATG5, ATG12, ATG3, RAB7, and LC3 type II: type I as normalized to GAPDH (C). Significance was determined using a student *t* test with *P*-value < 0.05. Data are means  $\pm$  SEM (*n* = 24/treatment for cell viability and *n*=3 for immunoblot) and the figure is a representative immunoblot for at least 2 independent experiments. \* indicates significant difference between control and infected cells. Abbreviation: hFOB, human fetal osteoblast; MTT, 3-(4,5-dimethylthiazol-2-yl)-2,5-diphenyl tetrazolium bromide; MOI, multiplicity of infection.

(Xie et al., 2016). Decreased protein and gene expression of these key elongation factors could contribute to BCO pathogenicity.

The fusion of the fully formed autophagosome with the lysosome and subsequent maturation of the autolysosome involves the Rab-SNARE (Soluble NSF Attachment Proteins Receptor) system including Ras-related protein Rab-7a (RAB7A) (Nakamura and Yoshimori, 2017; Kuchitsu and Fukuda, 2018; Kuchitsu et al., 2018). RAB7A is responsible for the transport of autophagosomes along microtubules for proceeding fusion via interaction with specific effectors (Pankiv et al., 2010; Nakamura and Yoshimori, 2017). In BCO-affected bone, RAB7A mRNA expression was significantly downregulated indicating potential dysregulation of this key fusion machinery.

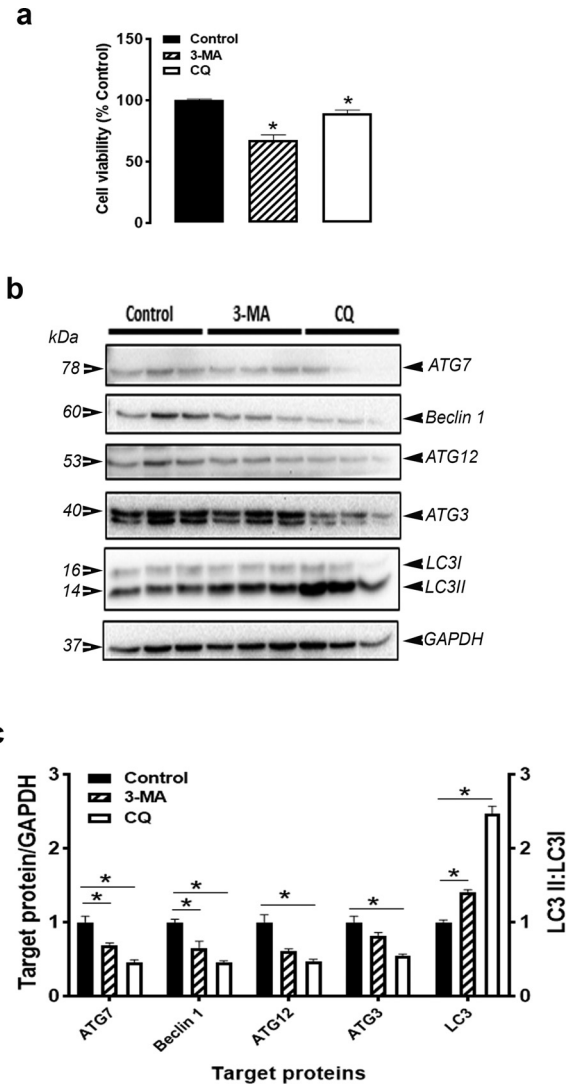


**Figure 6.** Effect of autophagy inhibition via 3-MA and CQ on cell viability and autophagy machinery in hFOB cells. MTT assay for cell viability presented as percent of control viability under treatment of 3-MA (5 mM), CQ (10  $\mu$ M), or a vehicle control on hFOB cells for 24 h (A). Western blot results for autophagy machinery proteins (B) and statistical analysis for ATG7, Beclin1, ATG12, ATG3, and LC3 type II: type I as normalized to GAPDH (C). Significance was determined using One-way ANOVA with *P*-value < 0.05. Data are means  $\pm$  SEM (*n* = 24/treatment for cell viability and *n*=3 for immunoblot) and the figure is a representative immunoblot for at least 2 independent experiments. \* indicates significant difference compared to the control (untreated) cells. Abbreviations: 3-MA, 3-methyladenine; CQ, chloroquine; hFOB, human fetal osteoblast

Taken as a whole, the *in vivo* results of this study suggest a dysregulation of key machinery in every stage of autophagy in BCO-affected tissue. In order to determine if this dysregulation was a direct result of the bacterial component of BCO, an *in vitro* experiment was conducted with hFOB cells and known BCO isolate, *S. agnetis* 908. Not only did challenged cells show significant decreased viability, but also similar autophagy machinery dysregulation resulting from bacterial challenge. Key initiation protein Beclin1, as well as elongation machinery, ATG7, ATG16L, ATG12, and ATG3, were significantly decreased in *S. agnetis*-infected hFOB cells. Most notably, the ratio of LC3 type I to LC3 type II significantly increased under bacterial challenge. LC3

has been used as an indicator of autophagy function with the accumulation of LC3 type II in relation to LC3 type I occurring due to lack of LC3 type II lysosomal degradation when autophagy is dysregulated (Ushio et al., 2011; Girolamo et al., 2019). These results could be indicative of a potential decrease in autophagic activity in bacterially challenged cells. In bone tissue, autophagy is essential in osteoblast differentiation with suppression of autophagy also playing a role in decreased cellular function via reduced autophagic vacuoles containing apatite crystals inhibiting mineralization (Li et al., 2018).

To elucidate whether autophagy inhibition has a direct effect, 2 different autophagy inhibitors were used, 3-MA and CQ. 3-MA inhibits class II PI3Ks thereby inhibiting autophagy, primarily in the nucleation stage (Zhang et al., 2021). While CQ inhibits autophagy via blocking of lysosomal function and thereby acting on the fusion stage (Pasquier, 2016; Galluzzi et al., 2017). Both treatments resulted in significant decreased hFOB cell viability and increased ratio of LC3 type II to type I. Additionally, decreased expression of ATG7 and Beclin1 was also seen in cells treated with 3-MA and cells treated with CQ. ATG12 and ATG3 protein was significantly lower in CQ-treated cells compared to control. These results suggest that inhibition of autophagy, in either earlier or later stages, results in decreased cell viability comparable to that seen when cells are challenged with a known BCO isolate.

Taken together, the results from this study are the first to implicate autophagy machinery dysregulation in the pathogenicity of BCO in modern broilers. While more research into the exact mechanism and machinery involved in BCO is needed, clearly, autophagy machinery dysregulation is present in BCO and could be caused by bacterial infection. This dysregulation has the capacity to reduce cell viability and potentially contribute to the etiology and symptoms of BCO. These findings give a new perspective into potential targets for treatment and prevention of BCO via genetics, probiotics, or pharmacological means.

## DISCLOSURES

The authors declare no conflicts of interest.

## REFERENCES

- Abeliovich, H., W. A. Dunn, J. Kim, and D. J. Klionsky. 2000. Dissection of autophagosome biogenesis into distinct nucleation and expansion steps. *J. Cell Biol.* 151:1025–1033.
- Al-Rubaye, A. A. K., M. B. Couger, S. Ojha, J. F. Pummill, J. A. Koon 2nd, R. F. Wideman Jr., and D. D. Rhoads. 2015. Genome analysis of *Staphylococcus agnetis*, an agent of lameness in broiler chickens. *PLoS One* 10 e0143336-e0143336.
- Alrubaye, A. A. K., N. S. Ekesi, A. Hasan, E. Elkins, S. Ojha, S. Zaki, S. Dridi, R. F. Wideman, M. A. Rebollo, and D. D. Rhoads. 2020. Chondronecrosis with osteomyelitis in broilers: further defining lameness-inducing models with wire or litter flooring to evaluate protection with organic trace minerals. *Poultry Sci.* 99:5422–5429.
- Amano, A., I. Nakagawa, and T. Yoshimori. 2006. Autophagy in innate immunity against intracellular bacteria. *J Biochem-Tokyo* 140:161–166.
- Birmingham, C. L., A. C. Smith, M. A. Bakowski, T. Yoshimori, and J. H. Brumell. 2006. Autophagy controls salmonella infection in response to damage to the salmonella-containing vacuole. *J. Biol. Chem.* 281:11374–11383.
- Carter, L. E., G. Kilroy, J. M. Gimble, and Z. E. Floyd. 2012. An improved method for isolation of RNA from bone. *BMC Biotechnol.* 12:5.
- Cemma, M., and JH. Brumell. 2012. Interactions of pathogenic bacteria with autophagy systems. *Curr. Biol.* 22:R540–R545.
- Chu, Y., Y. Kang, C. Yan, C. Yang, T. Zhang, H. Huo, and Y. Liu. 2020. LUBAC and OTULIN regulate autophagy initiation and maturation by mediating the linear ubiquitination and the stabilization of ATG13. *Autophagy* 17:1684–1699.
- Deretic, V., T. Saitoh, and S. Akira. 2013. Autophagy in infection, inflammation and immunity. *Nat. Rev. Immunol* 13:722–737.
- Desantis, A., T. Bruno, V. Catena, F. De Nicola, F. Goeman, S. Iezzi, C. Sorino, M. Ponzoni, G. Bossi, V. Federico, F. La Rosa, M. R. Ricciardi, E. Lesma, P. D. O. De Meo, T. Castrignano, M. T. Petrucci, F. Pisani, M. Chesi, P. L. Bergsagel, A. Floridi, G. Tonon, C. Passananti, G. Blandino, and M. Fanciulli. 2015. Che-1-induced inhibition of mTOR pathway enables stress-induced autophagy. *EMBO J.* 34:1214–1230.
- Döring, T., L. Zeyen, C. Bartusch, and R. Prange. 2018. Hepatitis B virus subverts the autophagy elongation complex Atg5-12/16L1 and does not require Atg8/LC3 lipidation for viral maturation. *J. Virol.* 92:e01513-17.
- Drudi, S., Y. Hirano, V. Tarallo, Y. Kim, B. J. Fowler, B. K. Ambati, S. Bogdanovich, V. A. Chiodo, W. W. Hauswirth, J. F. Kugel, J. A. Goodrich, S. L. Ponicsan, D. R. Hinton, M. E. Kleinman, J. Z. Baffi, B. D. Gelfand, and J. Ambati. 2012. ERK1/2 activation is a therapeutic target in age-related macular degeneration. *P. Natl. Acad. Sci.* 109:13781–13786.
- Esteves, A. R., F. Filipe, J. D. Magalhães, D. F. Silva, and S. M. Cardoso. 2019. The role of Beclin-1 acetylation on autophagic flux in Alzheimer's disease. *Mol. Neurobiol.* 56:5654–5670.
- Ferver, A., E. Greene, R. Wideman, and S. Dridi. 2021. Evidence of mitochondrial dysfunction in bacterial chondronecrosis with osteomyelitis-affected broilers. *Front. Vet. Sci.* 8:640901.
- Galluzzi, L., J. M. Bravo-San Pedro, B. Levine, D. R. Green, and G. Kroemer. 2017. Pharmacological modulation of autophagy: therapeutic potential and persisting obstacles. *Nat. Rev. Drug Discov.* 16:487–511.
- Geng, N., X. Wang, X. Yu, R. Wang, Y. Zhu, M. Zhang, J. Liu, and Y. Liu. 2020. *Staphylococcus aureus* avoids autophagy clearance of bovine mammary epithelial cells by impairing lysosomal function. *Front. Immunol.* 11 746-746.
- Greene, E., J. Flees, A. Dhamad, A. Alrubaye, S. Hennigan, J. Pleimann, M. Smeltzer, S. Murray, J. Kugel, J. Goodrich, A. Robertson, R. Wideman, D. Rhoads, and S. Dridi. 2019. Double-stranded RNA is a novel molecular target in osteomyelitis pathogenesis a translational avian model for human bacterial chondronecrosis with osteomyelitis. *Am. J. Pathol.* 189:2077–2089.
- Han, Z., W. Wang, X. Lv, Y. Zong, S. Liu, Z. Liu, L. Wang, and L. Song. 2019. ATG10 (autophagy-related 10) regulates the formation of autophagosome in the anti-virus immune response of pacific oyster (*Crassostrea gigas*). *Fish Shellfish Immun.* 91:325–332.
- He, C., H. Song, T. Yorimitsu, I. Monastyrska, W.-L. Yen, J. E. Legakis, and D. J. Klionsky. 2006. Recruitment of Atg9 to the preautophagosomal structure by Atg11 is essential for selective autophagy in budding yeast. *J. Cell Biol.* 175:925–935.
- Houtman, J., K. Freitag, N. Kimber, J. Schmoranzner, F. L. Heppner, and M. Jendrach. 2019. Beclin1-driven autophagy modulates the inflammatory response of microglia via NLRP3. *EMBO J.* 38 n/a-n/a.
- Hurley, J. H., and L. N. Young. 2017. Mechanisms of autophagy initiation. *Annu. Rev. Biochem.* 86:225–244.
- Ichimiya, T., T. Yamakawa, T. Hirano, Y. Yokoyama, Y. Hayashi, D. Hirayama, K. Wagatsuma, T. Itoi, and H. Nakase. 2020. Autophagy and autophagy-related diseases: a review. *Int. J. Mol. Sci.* 21:8974.
- Kageyama, S., H. Omori, T. Saitoh, T. Sone, J.-L. Guan, S. Akira, F. Imamoto, T. Noda, and T. Yoshimori. 2011. The LC3

- recruitment mechanism is separate from Atg9L1-dependent membrane formation in the autophagic response against Salmonella. *Mol. Biol. Cell* 22:2290–2300.
- Ke, D., L. Ji, Y. Wang, X. Fu, J. Chen, F. Wang, D. Zhao, Y. Xue, X. Lan, and J. Hou. 2019. JNK1 regulates RANKL-induced osteoclastogenesis via activation of a novel Bcl-2-Beclin1-autophagy pathway. *FASEB J.* 33:11082–11095.
- Kishi-Itakura, C., I. Koyama-Honda, E. Itakura, and N. Mizushima. 2014. Ultrastructural analysis of autophagosome organization using mammalian autophagy-deficient cells. *J. Cell Sci.* 127:4089–4102.
- Klionsky, D. J. 2005. Autophagy. *Curr Biol.* 15:R282–R283.
- Kotani, T., H. Kirisako, M. Koizumi, Y. Ohsumi, and H. Nakatogawa. 2018. The Atg2-Atg18 complex tethers pre-autophagosomal membranes to the endoplasmic reticulum for autophagosome formation. *P. Natl. Acad. Sci.* 115:10363–10368.
- Kuchitsu, Y., and M. Fukuda. 2018. Revisiting Rab7 functions in mammalian autophagy: Rab7 knockout studies. *Cells.* 7:215.
- Kuchitsu, Y., Y. Homma, N. Fujita, and M. Fukuda. 2018. Rab7 knockout unveils regulated autolysosome maturation induced by glutamine starvation. *J. Cell Sci.* 131:jcs215442.
- Kuma, A., A. Yamamoto, M. Hatano, T. Tokuhiisa, T. Yoshimori, N. Mizushima, Y. Ohsumi, M. Matsui, and H. Nakaya. 2004. The role of autophagy during the early neonatal starvation period. *Nature* 432:1032–1036.
- Li, H., D. Li, Z. Ma, Z. Qian, X. Kang, X. Jin, F. Li, X. Wang, Q. Chen, H. Sun, and S. Wu. 2018. Defective autophagy in osteoblasts induces endoplasmic reticulum stress and causes remarkable bone loss. *Autophagy* 14:1726–1741.
- Li, X., J. Yan, L. Wang, F. Xiao, Y. Yang, X. Guo, and H. Wang. 2013. Beclin1 inhibition promotes autophagy and decreases gemcitabine-induced apoptosis in Miapaca2 pancreatic cancer cells. *Cancer Cell Int.* 13 26–26.
- Liu, Y.-J., L. Zhang, C. J. Pappasian, and H.-W. Deng. 2014. Genome-wide association studies for osteoporosis: a 2013 update. *J. Bone Metab.* 21:99–116.
- Lv, Y., L. Fang, P. Ding, and R. Liu. 2019. PI3K/Akt-Beclin1 signaling pathway positively regulates phagocytosis and negatively mediates NF- $\kappa$ B-dependent inflammation in *Staphylococcus aureus*-infected macrophages. *Biochem. Bioph. Res. Co.* 510:284–289.
- Matsunaga, K., E. Morita, T. Saitoh, S. Akira, N. T. Ktistakis, T. Izumi, T. Noda, and T. Yoshimori. 2010. Autophagy requires endoplasmic reticulum targeting of the PI3-kinase complex via Atg14L. *J. Cell Biol.* 190:511–521.
- Maurer, K., T. Reyes-Robles, F. Alonzo, J. Durbin, V. J. Torres, and K. Cadwell. 2015. Autophagy mediates tolerance to *Staphylococcus aureus* Alpha-Toxin. *Cell Host Microbe.* 17:429–440.
- Mei, Y., M. Su, R. Sanishvili, S. Chakravarthy, C. L. Colbert, and S. C. Sinha. 2016. A. I. L. Argone National Lab. 2016. Identification of BECN1 and ATG14 Coiled-Coil Interface Residues That Are Important for Starvation-Induced Autophagy. *Biochem* 55:4239–4253.
- Nair, U., A. Jotwani, J. Geng, N. Gammoh, D. Richerson, W.-L. Yen, J. Griffith, S. Nag, K. Wang, T. Moss, M. Baba, J. A. McNew, X. Jiang, F. Reggiori, T. J. Melia, and Daniel J. Klionsky. 2011. SNARE proteins are required for macroautophagy. *Cell.* 146:290–302.
- Nakamura, S., and T. Yoshimori. 2017. New insights into autophagosome-lysosome fusion. *J. Cell Sci.* 130:1209–1216.
- Neumann, Y., S. A. Bruns, M. Rohde, T. K. Prajsnar, S. J. Foster, and I. Schmitz. 2016. Intracellular *Staphylococcus aureus* eludes selective autophagy by activating a host cell kinase. *Autophagy* 12:2069–2084.
- Noda, T., N. Fujita, and T. Yoshimori. 2009. The late stages of autophagy: how does the end begin? *Cell Death Differ.* 16:984–990.
- Obara, K., and Y. Ohsumi. 2011. Atg14: a key player in orchestrating autophagy. *Int. J. Cell Biol.* 2011:713435–713437.
- Obara, K., T. Sekito, K. Niimi, and Y. Ohsumi. 2008. Atg18-Atg2 complex is recruited to autophagic membranes via phosphatidylinositol 3-Phosphate and exerts an essential function. *J. Biol. Chem.* 283:23972–23980.
- Ogawa, M., H. Mimuro, Y. Yoshikawa, H. Ashida, and C. Sasakawa. 2011. Manipulation of autophagy by bacteria for their own benefit. *Microbiol. Immunol.* 55:459–471.
- Onal, M., M. Piemontese, J. Xiong, Y. Wang, L. Han, S. Ye, M. Komatsu, M. Selig, R. S. Weinstein, H. Zhao, R. L. Jilka, M. Almeida, S. C. Manolagas, and C. A. O'Brien. 2013. Suppression of autophagy in osteocytes mimics skeletal aging. *J. Biol. Chem.* 288:17432–17440.
- Pankiv, S., E. A. Alemu, A. Brech, J.-A. Bruun, T. Lamark, A. Øvervatn, G. Bjørkøy, and T. Johansen. 2010. FYCO1 is a Rab7 effector that binds to LC3 and PI3P to mediate microtubule plus end-directed vesicle transport. *J. Cell Biol.* 188:253–269.
- Pasquier, B. 2016. Autophagy inhibitors. *Cell. Mol. Life Sci.* 73:985–1001.
- Piekarski, A., S. Khaldi, E. Greene, K. Lassiter, J. G. Mason, N. Anthony, W. Bottje, and S. Dridi. 2014. Tissue distribution, gender- and genotype-dependent expression of autophagy-related genes in avian species. *PLoS One* 9 e112449–e112449.
- Piekarski, A., G. Nagarajan, P. Ishola, J. Flees, E. S. Greene, W. J. Kuenzel, T. Ohkubo, H. Maier, W. G. Bottje, M. A. Cline, and S. Dridi. 2018. AMP-Activated protein kinase mediates the effect of leptin on avian autophagy in a tissue-specific manner. *Front. Physiol.* 9:541.
- Piekarski-Welsler, A., E. Greene, K. Lassiter, B. C. Kong, S. Dridi, and W. Bottje. 2018. Enrichment of autophagy and proteasome pathways in breast muscle of feed efficient pedigree male broilers. *Front. Physiol.* 9 1342–1342.
- Piemontese, M., M. Onal, J. Xiong, L. Han, J. D. Thostenson, M. Almeida, and C. A. O'Brien. 2016. Low bone mass and changes in the osteocyte network in mice lacking autophagy in the osteoblast lineage. *Sci. Rep.-UK* 6 24262–24262.
- Sawa-Makarska, J., V. Baumann, N. Coudevylle, S. von Bulow, V. Nogellova, C. Abert, M. Schuschnig, M. Graef, G. Hummer, and S. Martens. 2020. Reconstitution of autophagosome nucleation defines Atg9 vesicles as seeds for membrane formation. *Science* 369:1206.
- Schmittgen, T. D., and K. J. Livak. 2008. Analyzing real-time PCR data by the comparative C(T) method. *Nat. Protoc.* 3:1101–1108.
- Schnaith, A., H. Kashkar, S. A. Leggio, K. Addicks, M. KrÄ¼nke, and O. Krut. 2007. *Staphylococcus aureus* subvert autophagy for induction of caspase-independent host cell death. *J. Biol. Chem.* 282:2695–2706.
- Shapiro, I. M., R. Layfield, M. Lotz, C. Settembre, and C. Whitehouse. 2014. Boning up on autophagy: the role of autophagy in skeletal biology. *Autophagy* 10:7–19.
- Shen, G., H. Ren, Q. Shang, T. Qiu, X. Yu, Z. Zhang, J. Huang, W. Zhao, Y. Zhang, D. Liang, and X. Jiang. 2018. Autophagy as a target for glucocorticoid-induced osteoporosis therapy. *Cell. Mol. Life Sci.* 75:2683–2693.
- Suzuki, K., Y. Kubota, T. Sekito, and Y. Ohsumi. 2007. Hierarchy of Atg proteins in pre-autophagosomal structure organization. *Genes Cells* 12:209–218.
- Ushio, H. P., T. P. Ueno, Y. P. Kojima, M. P. Komatsu, S. P. Tanaka, A. P. Yamamoto, Y. P. Ichimura, J. P. Ezaki, K. P. Nishida, S. B. D. Komazawa-Sakon, F. P. Niyonsaba, T. P. Ishii, T. D. D. S. M. D. P. Yanagawa, E. M. D. P. Kominami, H. M. D. P. Ogawa, K. M. D. P. Okumura, and H. M. D. P. Nakano. 2011. Crucial role for autophagy in degranulation of mast cells. *J. Allergy Clin. Immun.* 127:1267–1276.e1266.
- Velikkakath, A. K. G., T. Nishimura, E. Oita, N. Ishihara, and N. Mizushima. 2012. Mammalian Atg2 proteins are essential for autophagosome formation and important for regulation of size and distribution of lipid droplets. *Mol. Biol. Cell* 23:896–909.
- Wang, L., B. L. Heckmann, X. Yang, and H. Long. 2019. Osteoblast autophagy in glucocorticoid-induced osteoporosis. *J. Cell. Physiol.* 234:3207–3215.
- Wideman, R. F., K. R. Hamal, J. M. Stark, J. Blankenship, H. Lester, K. N. Mitchell, G. Lorenzoni, and I. Pevzner. 2012. A wire-flooring model for inducing lameness in broilers: evaluation of probiotics as a prophylactic treatment. *Poultry Sci* 91:870–883.
- Wideman, R. F., and R. D. Prissy. 2012. Bone circulatory disturbances in the development of spontaneous bacterial chondronecrosis with osteomyelitis: a translational model for the pathogenesis of femoral head necrosis. *Front Endocrinol* 3:183.
- Wideman, R. 2015. Bacterial chondronecrosis with osteomyelitis and lameness in broilers: a review. *Poult Sci* 95.
- Xie, K., C. Liang, Q. Li, C. Yan, C. Wang, Y. Gu, M. Zhu, F. Du, H. Wang, J. Dai, X.a. Liu, G. Jin, H. Shen, H. Ma, and

- Z. Hu. 2016. Role of ATG10 expression quantitative trait loci in non-small cell lung cancer survival. *Int. J. Cancer* 139:1564–1573.
- Xie, Z., U. Nair, and D. J. Klionsky. 2008. Atg8 controls phagophore expansion during autophagosome formation. *Mol. Biol. Cell* 19:3290–3298.
- Yamamoto, H., Y. Fujioka, Sho W. Suzuki, D. Noshiro, H. Suzuki, C. Kondo-Kakuta, Y. Kimura, H. Hirano, T. Ando, Nobuo N. Noda, and Y. Ohsumi. 2016. The Intrinsically disordered protein Atg13 mediates supramolecular assembly of autophagy initiation complexes. *Dev. Cell* 38:86–99.
- Zachari, M., and I. G. Ganley. 2017. The mammalian ULK1 complex and autophagy initiation. *Essays Biochem.* 61:585–596.
- Zhang, X., L. Zhang, Y. Bi, T. Xi, Z. Zhang, Y. Huang, Y. Y. Lu, X. Liu, S. Shu, and F. Fang. 2021. Inhibition of autophagy by 3-methyladenine restricts murine cytomegalovirus replication. *J. Med. Virol.* 93:5001–5016.
- Zheng, L. W., W. C. Wang, X. Z. Mao, Y. H. Luo, Z. Y. Tong, and D. Li. 2020. TNF- $\alpha$  regulates the early development of avascular necrosis of the femoral head by mediating osteoblast autophagy and apoptosis via the p38 MAPK/NF- $\kappa$ B signaling pathway. *Cell Biol. Int.* 44:1881–1889.
- Zhuang, X., K. P. Chung, Y. Cui, W. Lin, C. Gao, B.-H. Kang, and L. Jiang. 2017. ATG9 regulates autophagosome progression from the endoplasmic reticulum in Arabidopsis. *P. Natl. Acad. Sci.* 114: E426–E435.